0273-2289/01/91–93/0387/$14.50

Measurement of Bubble Size Distribution in Protein Foam Fractionation Column Using Capillary Probe with Photoelectric Sensors

Liping Du, Yuqing Ding, Aleš Prokop, and Robert D. Tanner*

Chemical Engineering Department, Vanderbilt University, Nashville, TN 37235, E-mail: rtanner@vuse.vanderbilt.edu

Abstract

Bubble size is a key variable for predicting the ability to separate and concentrate proteins in a foam fractionation process. It is used to characterize not only the bubble-specific interfacial area but also coalescence of bubbles in the foam phase. This article describes the development of a photoelectric method for measuring the bubble size distribution in both bubble and foam columns for concentrating proteins. The method uses a vacuum to withdraw a stream of gas-liquid dispersion from the bubble or foam column through a capillary tube with a funnel-shaped inlet. The resulting sample bubble cylinders are detected, and their lengths are calculated by using two pairs of infrared photoelectric sensors that are connected with a high-speed data acquisition system controlled by a microcomputer. The bubble size distributions in the bubble column 12 and 1 cm below the interface and in the foam phase 1 cm above the interface are obtained in a continuous foam fractionation process for concentrating ovalbumin. The effects of certain operating conditions such as the feed protein concentration, superficial gas velocity, liquid flow rate, and solution pH are investigated. The results may prove to be helpful in understanding the mechanisms controlling the foam fractionation of proteins.

Index Entries: Bubble size; capillary tube; photoelectric method; foam fractionation; ovalbumin.

Introduction

Information about bubble size distributions is important to mass transfer, heat transfer, and chemical reaction, which are very dependent on the

*Author to whom all correspondence and reprint requests should be addressed.

interfacial area in many types of chemical processing equipment, such as stirred-tank reactors and distillation columns *(1–7)*. Bubble size distribution is also of paramount importance in a bubble or a foam column during a foam fractionation process, since this type of adsorptive separation technique depends on the specific gas bubble interfacial area, *a* (square centimeters of area/cubic centimeters of gas) *(8–11)*. The specific interfacial area relates to the bubble diameter. The area-to-volume relation between a single bubble and its specific surface area, *a*, is given by Eq. 1 for an ideal spherical bubble:

$$a = \frac{4\pi R^2}{(4/3)\pi R^3} = \frac{3}{R} = \frac{6}{d} \tag{1}$$

in which R and d are the bubble radius and diameter, each measured in centimeters, respectively. In the foam phase, each bubble cell is generally close to a dodecahedron in shape *(8)*; thus, Eq. 1 is often modified to the more-descriptive Eq. 2 *(8)*:

$$a = \frac{6.59}{d} \tag{2}$$

Equations 1 and 2 show that the smaller the bubble size, the larger the specific interfacial area of each bubble. Smaller bubbles lead to larger interfacial areas and, thus, adsorb more solute than do larger bubbles in a foam column. It follows then that the enrichment (the ratio of protein concentration of the foamate to the protein concentration of the initial solution), a measure of concentration/purification performance, will be higher for a foam column with smaller bubbles than a column with larger bubbles assuming that the gas fraction and surface concentration remain the same.

The rheology and stability of the foam are strongly influenced by the foam's bubble size distribution and gas-liquid fraction *(11)*. Therefore, to understand the foaming process, it is necessary to know the bubble size distribution and how that distribution affects the flow properties and is itself affected by flow processes in a foam *(10)*. For example, Brown et al.'s *(12)* study showed that large bubbles cause high drainage (liquid flow in liquid films and in plateau borders formed between the bubbles) flow rates and thinner liquid films. Subsequently, large bubbles are more prone to rupture (owing to their thinner liquid films) in a foam column and, thus, destabilize the foam *(12)*. The increase in bubble size along the length of a foam column reflects the degree of bubble coalescence (two small bubbles become one large bubble because the film between them breaks) in the foam phase *(8,9,11,12)*.

Coalescence in a foam column cannot now be predicted from theory *(9)*. Therefore, the development of the proposed photoelectric capillary probe method may provide appropriate measurements of the bubble size distribution, which, in turn, can contribute empirical information on bubble coalescence needed for modeling a foam column *(9)*. Generally, bubble size is affected by solution and gas-liquid surface properties, such

as solution pH, protein concentration, surface viscosity, surface tension, and some operating parameters, such as the superficial gas velocity and size of the sparger *(8,9,12,13)*.

Presently, the bubble size in a gas-liquid dispersion system can be determined by direct and indirect methods *(1)*. Indirect methods include the interfacial area method and the chemical method. These techniques give only the average bubble size in an entire system and cannot give either local or distribution information *(1)*. A direct photographic method is tedious and usually does not provide very high accuracy. A conductivity method only can give global information of liquid fraction *(14)*. The capillary probe (with a photoelectric sensor) method, however, can be developed to obtain the bubble size distribution directly in order to determine the bubble size distributions of the fermentation media *(2)*, a stirred-tank reactor *(1)*, and a stirred large-scale vessel *(3)*. Bae and Tavlarides *(15)* used a laser capillary spectrophotometer for the measurement of drop size distribution of reactive liquid-liquid dispersions. Research conducted in China *(4–7)* also independently included the use of the capillary photoelectric method for bubble size measurement in stirred gas-liquid dispersion systems. The capillary probe method, which uses a capillary probe and photoelectric sensors, combined with a high-speed microcomputer data acquisition system, can perform online measurements and give information on local bubble size distribution relatively quickly. To date, studies using this measurement method have focused on nonfoaming gas-liquid dispersions with large liquid holdups (>20%) *(1–7)* or liquid-liquid dispersions *(15)*.

Reports of bubble size distribution measurements in foam columns (liquid holdup <10%) are not common in the literature. The photography method has been used by Wong et al. *(13)* and Brown et al. *(12)* to obtain information on bubble size distribution in a foam column. However, a disadvantage of the photography method is that the measured two-dimensional picture reflects only the bubble size information on a transparent surface, which may be different from the actual bubble size information present inside a three-dimensional foam.

In this article, we describe our early work with the photoelectric capillary probe method in the foam column (liquid holdup <10%), in addition to the bubble column during foam fractionation of ovalbumin. It is apparently the first time that such measurements of bubble size in a foam column (near the interface with the bubble column) have been reported. Our measurement technique is similar to those previously reported in the literature *(1–7,15)* except that we use a pair of infrared phototransistors to obtain bubble signals within a capillary.

Principles of Photoelectric Suction Probe Method

The basic principle of the photoelectric suction probe method is that a bubble is reshaped into a cylindrical slug within a fine glass capillary probe when the bubble is sucked into the tube *(1)*. In the subsequent analysis, it is assumed that the bubble slug is uniform and occupies the whole

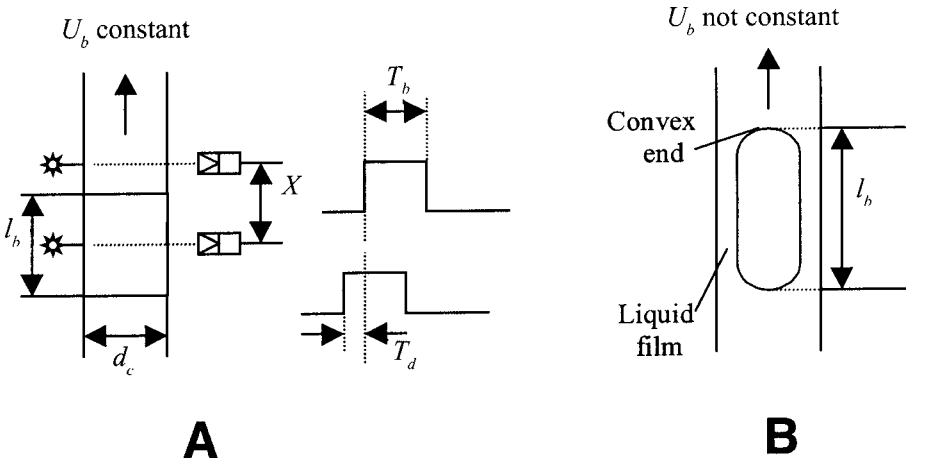

Fig. 1. Schematic of photoelectric method **(A)** and bubble flow inside a capillary **(B)** *(3)*.

cross section of the capillary and moves at constant velocity, U_b (Fig. 1A). Using these assumptions, the individual bubble length, l_b, and equivalent spherical diameter, d, can be determined by Eqs. 4 and 5. Equation 3 yields the bubble velocity, U_b, which is the quotient of distance and time:

$$U_b = X/T_d \tag{3}$$

$$l_b = U_b/T_b \tag{4}$$

$$d = \left[\frac{\pi l_b \left(\frac{d_c}{2} \right)^2}{\frac{1}{6}\pi} \right]^{1/3} = \left(\frac{3XT_b d_c^2}{2T_d} \right)^{1/3} \tag{5}$$

Here, X is the distance between two pairs of photoelectric sensors, d_c is the inside diameter of the capillary, T_d is the time it takes a bubble to travel the distance X, and T_b is the time it takes a whole bubble to pass through one sensor (as shown in Fig. 1A). Equation 5 results from equating the bubble volume to the cylinder volume in the capillary.

The Sauter mean diameter of the bubble size distribution, d_{32}, is then obtained (Eq. 6) *(1)*:

$$d_{32} = \frac{\sum_{i=1}^{N} d_i^3}{\sum_{i=1}^{N} d_i^2} \tag{6}$$

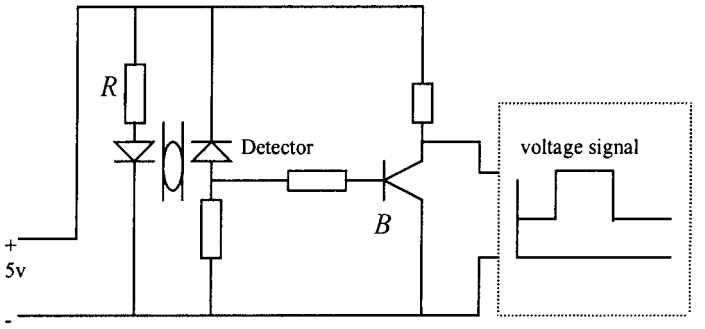

Fig. 2. Schematic of electric circuit.

in which N is the total number of bubbles sampled and d_i is the individual bubble diameter measured.

With the measured total time applied, the void fraction can now be calculated using Eq. 7:

$$\varepsilon_g = \frac{\sum_{i=1}^{N} T_{b,i}}{t_{\text{total}}} \tag{7}$$

Equation 7 assumes that the thickness of the bubble wall is negligible and bubble velocity, U_b, is constant.

On the right-hand sides of Eqs. 5 and 7, the only unknown values are T_b and T_d. In the photoelectric capillary probe method, T_b and T_d are measured and recorded automatically by the computer, with an installed high-speed data acquisition system. By applying a vacuum at the outlet of a capillary and immersing the other end into the gas-liquid dispersion system, a stream of the gas-liquid dispersion is sucked into the capillary and passed by two pairs of photoelectric sensors fixed in the apparatus surrounding the capillary. An electric circuit (Fig. 2) that connects the sensors will generate voltage signals whose magnitudes depend on which phase (liquid or gas) is detected. Typically, in a few seconds, several hundred bubbles pass by the sensors and the voltage signals are simultaneously recorded by the computer (Fig. 1). T_b and T_d are calculated from the time intervals between the gas and liquid phases (Fig. 1), thus obtaining the individual bubble diameters on line.

Theoretical Correction to Individual Bubble Size Measured in Capillary

Actual bubble flow in a capillary is very complex *(1–7,16)* and deviates from the ideal description in Fig. 1A, because bubble slugs flowing inside a capillary tube are under the action of several forces: buoyancy, pressure gradient, inertial force, liquid viscosity force between the wall and

the liquid film, and surface tension *(3)*. The actual shape of a bubble cylinder is not exactly an ideal cylinder because of its convex ends. Also, the cylinder does not occupy the whole cross section of the tube because of the thin liquid film surrounding the bubble (Fig. 1B). In addition, the volume of the cylinder may be different from the bubble volume in original dispersion owing to the expansion resulting from the pressure drop along the axis of the capillary. The velocity of the bubble is not constant along the capillary owing to the pressure gradient along its length. Even the tail velocity of a bubble slug can be different from its nose velocity *(3)*. Therefore, the volume of bubble measured in the capillary may be different from the true volume in the original dispersion, even though coalescence and breakup of slugs inside the tube are minimized when the suction pressure is in a suitable range *(4)*. To correct the volume error, either a direct calibration or a theoretical correction to the measured bubble size in the capillary is needed *(1–3)*.

Two-phase flow inside a capillary tube provides the theoretical basis for the correction of the measured bubble size in a capillary *(16)*. By neglecting the liquid film surrounding the bubble slug, Eq. 8 can be derived by equating the true bubble volume to the bubble slug volume (after pressure correction as ideal gas) in the capillary *(5)*:

$$d_b = \left(\frac{p}{p_0}\right)^{1/3} \left(\frac{3}{2}\frac{l_b}{d_c} - \frac{1}{2}\right)^{1/3} d_c \tag{8}$$

in which p is the pressure inside the capillary at the point where the bubble is detected. p is calculated from the pressure gradient equation based on two-phase flow inside a capillary tube. Yu et al. *(5)* found that when a capillary of 0.66-mm id was used with a vacuum of 40–53.3 kPa, the absolute error between the measured bubble diameter (after pressure correction) and the true value was <0.07 mm (a relative error <4.26%) for an individual surfactant bubble 1.0–3.0 mm in diameter. For the case in which the liquid film surrounding the bubble slug is not negligible, Zhang et al. *(7)* developed the bubble size correction formula as follows:

$$d_b = \left(\frac{3pl_b d_c^2}{2.38p_0}\right)^{1/3} = \left(\frac{p}{p_0}\right)^{1/3} \left(\frac{3l_b}{2.38d_c}\right)^{1/3} d_c \tag{9}$$

Equation 9 was obtained under the assumption of $S_k / S_b = 1.19$, in which S_k and S_b are cross-sectional areas of the capillary tube and bubble slug, respectively. This assumption is valid when Reynolds number is >3000 for plug flow (two phase) within a capillary *(16)*. Zhang et al.'s *(7)* simulation of the pressure drop along the length of the capillary tube showed that over a wide range of experimental conditions, the pressure drop is nearly linear with the length. Using a linear approximation to the pressure gradient and

Eq. 9, a 3% maximum deviation of bubble diameter (for the bubble range of 0.5–6 mm) from that obtained using a photographic method was observed with the photoelectric capillary probe method (1.8-mm diameter capillary).

Using a linear pressure drop along the axis of the capillary, considering the surrounding liquid film, Greaves and Kobbacy *(1)* developed a semiempirical formula for estimating the bubble volume (Eq. 10). Equation 10 showed a 30% on average overestimation of bubble volume (or 9% of diameter for 0.3- to 6-mm bubbles) over that calibrated by injecting a known volume bubble in the inlet of the capillary by a precision micrometer needle syringe *(1)*.

$$V_b = \frac{t_b^* U_b^* A}{P_A}\left[1 - \left(\frac{\mu U_b^*}{\sigma}\right)^{1/2}\right] \times \left[P_A - \frac{z}{l_c - t_b^* U_b^*}(P_A - P_V - 0.163\rho U_b^{*2})\right] \quad (10)$$

Equation 10 was applied in our work, along with the 9% overestimate correction for the spherical diameter (which was subtracted). We assume that the error of measured bubble diameter in our measurement will thus be <5%, because the diameter of the capillary tube we used, 0.5 mm, is very close to the 0.61 mm that Greaves and Kobbacy *(1)* used and the bubble dimensions in our bubble and foam column are close to those in his dispersion system (0.3–6 mm in diameter).

Improvement in Accuracy in Bubble Size Distribution

Even if the individual bubble size is measured accurately, the bubble size distribution results may be biased owing to the influence of sampling in a dynamic gas-liquid dispersion system. One problem is the coalescence or breakage that may occur at the inlet of the capillary. Another is the preferential attraction of bubbles of a certain size and liquid content into the capillary.

It has been established that the funnel-shaped capillary inlet tip could suppress the breakage of bubbles at the inlet of the capillary tube and that bubbles with radii smaller than the radius of curvature of the tip edge does not break on impact *(1–7)*. On the other hand, the funnel-shaped tip should not be too large; otherwise, significant disturbances of the two-phase flow pattern at the inlet would result. The tip size was therefore limited to suppress the breakage of the largest bubbles *(3)*. To minimize coalescence of bubbles at the inlet of the capillary, the residence time (on the order of milliseconds) of the bubbles at the inlet is shortened by increasing the suction velocity so that bubbles do not have enough time to coalesce (in milliseconds) before entering the capillary *(7)*. Greaves and Kobbacy *(1)* observed that a high sampling flow rate associated with a high suction velocity also minimizes the preferential attraction of specific size bubbles, thus making it possible for essentially all the bubbles around the sampling

area to be sucked into the tube in a given time. When the suction speed rose too high, however, the bubble slug velocity inside the capillary increased so much that the slug expansion in the flow direction became significant and bubble size accuracy was likely to be less. Therefore, suction velocity needs to be controlled in a suitable range. The measures of funnel-shaped inlet capillary and control of suction velocity have been demonstrated to be very useful in measuring the bubble size distribution in a high-liquid holdup dispersion system *(1–7)*.

In a low-liquid holdup (<10%) foam column system, strong bubble-bubble interactions cause difficulties in accurately maintaining bubble size distributions using the photoelectric capillary probe method. In such cases, bubble sizes tend to be large relative to those in the bubble column of the same foam fractionation column owing to coalescence, and the liquid films are thinner owing to drainage in the foam column. If the same sized capillary tip as that used in the bubble column is also used for measuring the foam, the breakage rate may increase when bubbles enter the capillary tube. If the same suction velocity as that of a bubble column is used, bubble slugs inside the capillary may expand so much that breakage or extreme strain occurs. Therefore, accurate bubble size distributions of very dry foams with big bubbles may not be easily obtained using the same capillary tube as that used for a bubble column.

Materials and Methods

Figure 3 shows the foam fractionation and bubble size experimental setup. Continuous foam fractionation experiments were carried out in the glass column (14-cm id, 50-cm length). In our experiments, air is pumped into the column at a certain flow rate (superficial gas velocity of 0.05–0.2 cm/s), through a porous sparger (pore size 40–60 μm) mounted flush to the column bottom. To minimize loss of water in the air effluent stream, air is passed through a humidifier before it enters the column. The inlet end of the capillary tube is submerged vertically in the bubble or foam column. Then a vacuum is applied to the outlet end to suck the sample into the capillary for measurement of bubble size. The interface between the bubble column and foam phase is defined here as position 0. The bubble column level was kept constant at 28 cm by equating the continuous input feed solution rate with the continuous output residue solution rate in order to obtain a steady state. Sampling occurred at two positions below the interface (referred to as –12 cm and –1 cm in the bubble column) and two positions above the interface (referred to as +1 cm and +21 cm) (Fig. 4). The airflow rate was controlled by a flow rate regulator, and the liquid feed input was varied by changing the speed of the liquid pump

The internal diameter of the capillary was selected to enable the smallest bubble to be detected—it was 0.5 mm. Bubbles slightly smaller than the capillary can still be transformed into short cylinders because of the liquid film surrounding the slug. The diameter of the funnel-shaped tip was

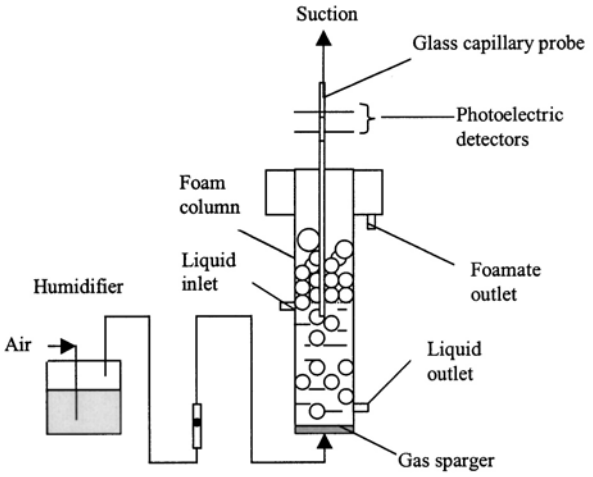

Fig. 3. Experimental setup of bubble size measurement and foam fractionation.

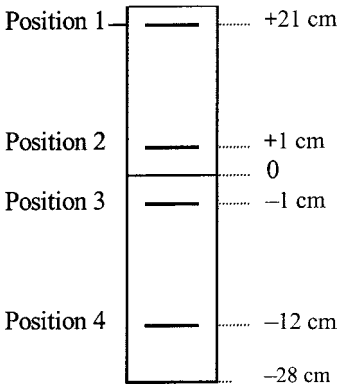

Fig. 4. Measurement points along the column. The 0 mark represents the interface between the bulk liquid phase (at the bottom) and the foam phase (at the top).

designed to be 6 mm based on our observation of bubble size in both the bubble and foam columns. The dimensions of the capillary tube are shown in Fig. 5. Two pairs of infrared photoelectric sensors, each of which comprises an infrared emitter and an infrared detector, were fixed (the distance between the two pairs of sensors is denoted as *X*) in the apparatus surrounding the capillary tube. At the position of each sensor pair, a very thin window was created by wrapping non-light-transparent material (here, TEFLON® tape) around the adjacent length along the capillary, in order to detect the very short slugs. The two-channel method was shown by Barigou and Greaves *(3)* to have low sensitivity to the velocity of bubbles inside the capillary. The vacuum pressure drop was controlled in a range of 1.5–1.75 psi (10.3–12.1 kPa) when the bubble size distribution in the bubble column was measured. This range was determined from our bubble size

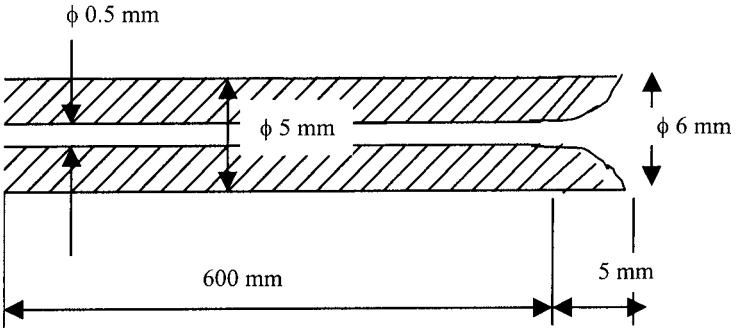

Fig. 5. Diagram of capillary probe (not to scale).

experiments at various vacuum pressure drops and to give the best relatively accurate results (unpublished data). Likewise, the vacuum pressure drop was determined to be optimal at 0.5 psi (3.45 kPa) when the foam column bubble size distribution was measured.

Protein (ovalbumin, grade II; Sigma, St. Louis, MO) aqueous solution was used in the foam fractionation experiments. It was prepared by dissolving ovalbumin powder into deionized water. Ovalbumin concentration was determined by the Coomassie blue method *(17)*. The pH of the solution was adjusted by adding 1.0 *M* NaOH or HCl solution as needed.

The measurement hardware, in addition to the capillary probe and photoelectric response circuit, included a PCI-6023E multifunction I/O board from National Instrument. The board was mounted inside a Gateway 2000 computer. Software included the Data Acquisition Driver Software from National Instrument, and we developed an application interface (Visual C) for measurement and data calculation and calibration (unpublished data).

Results and Discussion

Reproducibility

An important outcome of any experimental technique is the reproducibility of the results *(1,3–5)*. Figure 6 compares two consecutive measurements under the same conditions in the foam column (position +1 cm). Table 1 shows the average bubble size and void fraction results for these two runs. It is seen from both Fig. 6 and Table 1 that the photoelectric probe method used shows good reproducibility. Further investigation showed that a log normal distribution was adequate to represent the bubble size distribution data in Fig. 6 and all our other bubble size distribution data (unpublished data). The log normal distribution of the bubble size in a bubble or a foam column was also observed by Lage and Espósito *(18)*, Calvert and Nezhati *(10)*, and Wong et al. *(13)* using the photography method. This agreement showed at least that the sampling in our measure-

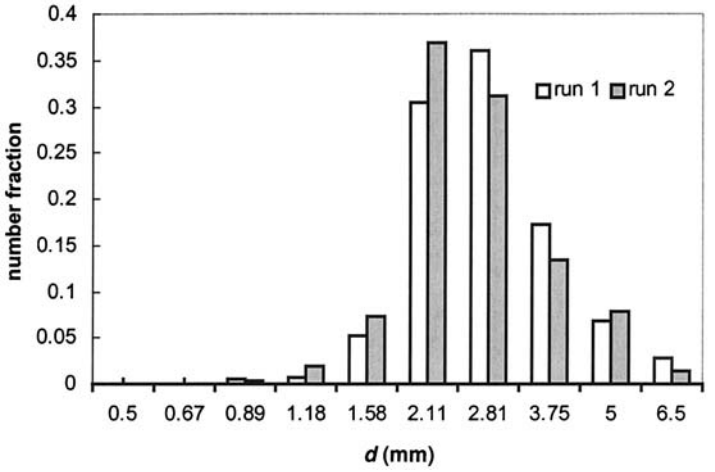

Fig. 6. Bubble size distribution at the bottom of the foam column (position +1 cm) under protein initial concentration of 56 mg/L, pH 9.7, superficial gas velocity of 0.1 cm/s, and liquid flow rate of 45 mL/min.

Table 1
Comparison of Two Measurement Results[a]

	Run 1	Run 2
Number of bubbles detected	418	453
Average bubble diameter (mm)		
By number	2.06	1.94
By surface area	2.16	2.04
By volume	2.28	2.15
Void fraction	0.89	0.90
Statistic average diameter (mm)	2.58	2.43
Deviation	1.02	0.87

[a]Bubble size distribution as Fig. 6.

ment is reliable and that the bubbles sampled are a good representation of those in bubble or a foam column.

Typical Bubble Size Distribution Results

Figure 7 shows the typical bubble size distribution results at two different positions: one in the bubble column just below (–1 cm) the interface, and the other in the foam column just above (+1 cm) the interface. We can see that below the surface, the bubble sizes are smaller and the bubble size distribution is narrower (deviation = 0.17), but above the surface, the bubbles become larger and the distribution is widened (deviation = 0.59). This change is attributed mainly to the coalescence of the bubbles at and above the interface (in the foam phase) *(19)*. The bubble size scale (0–5 mm) in Fig. 7 is in good agreement with the visual observation. Moreover, it is

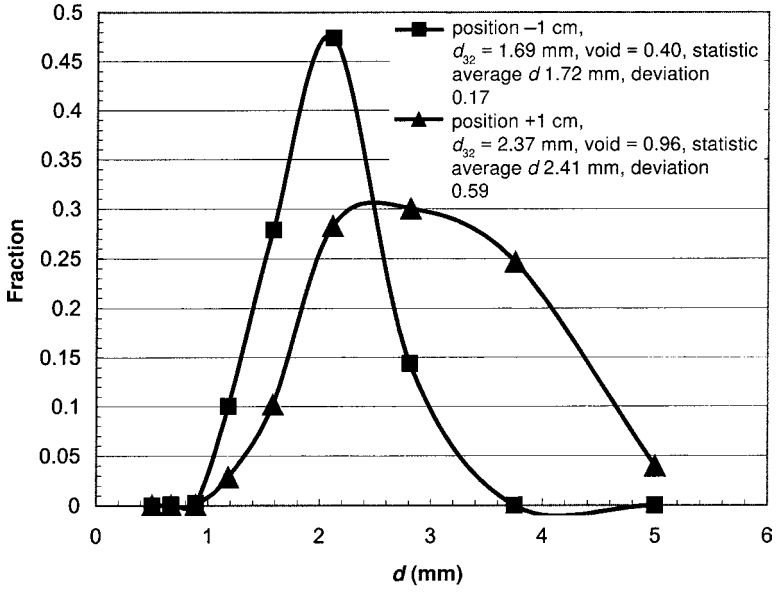

Fig. 7. Bubble size distribution at the top of the bulk liquid phase of bubble column and at the bottom of foam phase under protein initial concentration of 74.4 mg/L, pH 9.7, superficial gas velocity of 0.1 cm/s, and feed liquid flow rate of 45 mL/min.

close to the bubble size measured by Yu et al. *(5)*, Greaves and Kobbacy *(1)*, and Barigou and Greaves *(3)* in stirred gas-liquid dispersion systems using the photoelectric capillary probe method. It was also comparable to the bubble size measured by Lage and Espósito *(18)* in a similar bubble column, and Wong et al. *(13)* in a similar bovine serum albumin foam column using the photography method. In our previous work, the void fraction data obtained using the capillary probe method showed very good agreement with the weight method *(20)*, indicating that the capillary method used here is reasonably accurate and internally consistent.

Sauter Mean Diameter (d_{32}) and Void Fraction Variation with Position

Figure 8 shows the average bubble size, d_{32}, and the gas void fraction of gas change along the column. It can be seen that, in the bubble column, d_{32} and the void fraction grew gradually from position –12 cm to –1 cm. As the bubble crossed the interface, position 0, both d_{32} and the void fraction grew rapidly. In general, in a bubble column, the increase in the bubble size is mainly caused by the static pressure change at different liquid levels. For a very dilute solution, the density is approximately that of water. From position –12 cm to –1 cm, the static pressure decreases only slightly, so the bubble size change is negligible owing to this small static pressure change. When the bubbles rise up the bubble column to the interface, however, coalescence of some of these bubbles plays a significant role in the

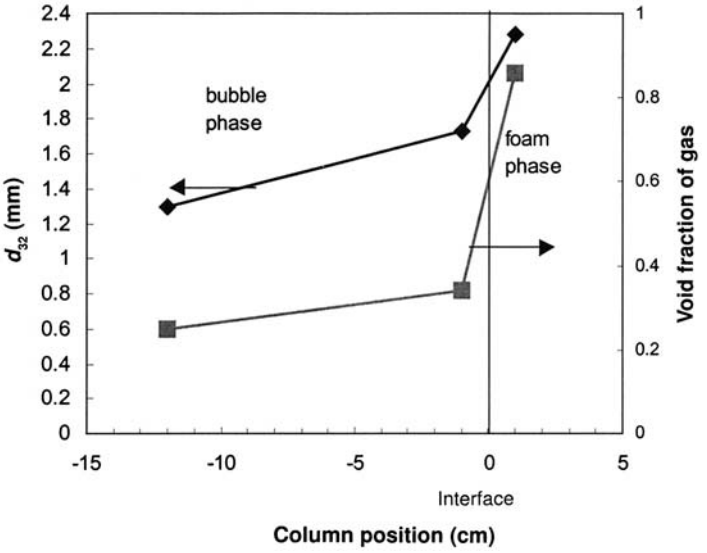

Fig. 8. Typical bubble size, d_{32}, and void fraction of the gas vs column position at an initial concentration of 35 mg/L, superficial gas velocity of 0.1 cm/s, and a liquid flow rate of 24 mL/min.

increase in bubble size. At the same time, because significant drainage occurs when the bubbles rise out of the bulk liquid phase, the void fraction increases rapidly. We were not able to accurately obtain the bubble size distribution at the top of the foam (+12 cm) using the same capillary tip owing to the very dry (liquid holdup <1%) foam and the large bubbles relative to the funnel-shaped inlet tip opening. Thus, the capillary tube and the method used here (without modification) were limited to measuring the bubble size only up to a low position in the foam column (such as 5 cm above the interface). Measuring the bubble sizes at higher positions needs to be investigated by enlarging the tip size and adjusting the vacuum pressure drop.

Sauter Mean Diameter (d_{32}) Varied with Protein Concentration

Figure 9 shows how d_{32} changes with the local ovalbumin concentration at the bubble column (position –1 cm). From the trend of the data, it is seen that as the ovalbumin increases in concentration, d_{32} decreases gradually and then levels off when the local protein concentration reaches 40 mg/L. This decrease in d_{32} can be explained by the surface concentration, Γ, which is a key variable in determining gas-liquid interfacial properties such as the surface viscosity and surface tension. The protein concentration (liquid) can be related to the surface concentration by an adsorption isotherm when the two variables are at equilibrium or by adsorption kinetics when they are not at equilibrium. If we assume that the surface concentration is at equilibrium with the protein liquid concentration in the form of a Langmuir isotherm, then with an increase in protein

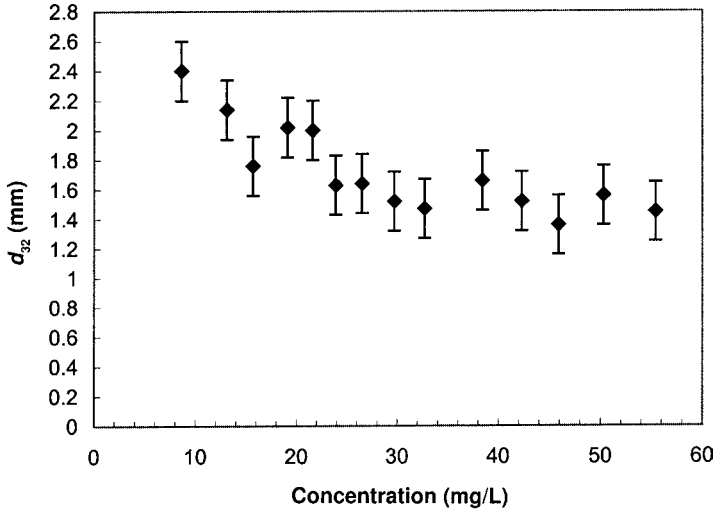

Fig. 9. Bubble diameter, d_{32}, vs local ovalbumin concentration at the higher position of the bubble column (position –1 cm) under superficial gas velocity of 0.1 cm/s, liquid flow rate of 24 mL/min, and pH 6.5 (original solution).

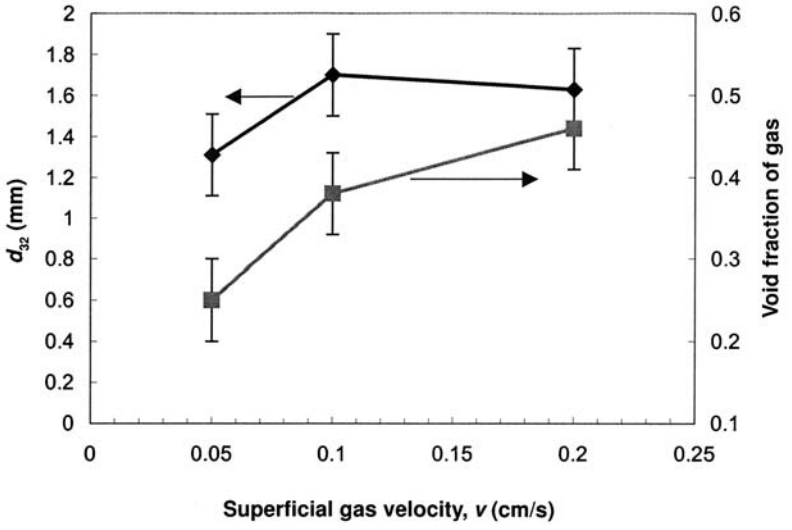

Fig. 10. Bubble size, d_{32}, and void fraction of gas vs superficial gas velocity at lower position of bubble column (position –12 cm) under initial ovalbumin concentration of 36.4 mg/L, liquid flow rate of 45 mL/min, and pH 6.5 (original solution).

concentration, the surface concentration increases. Once the protein liquid concentration reaches a given value, the surface concentration becomes saturated and will not increase further. Changes in surface tension will accompany changes in the surface concentration in an inverse relationship: the higher the surface concentration, the lower the surface tension. A lower surface tension may contribute to the formation of smaller bubbles. When

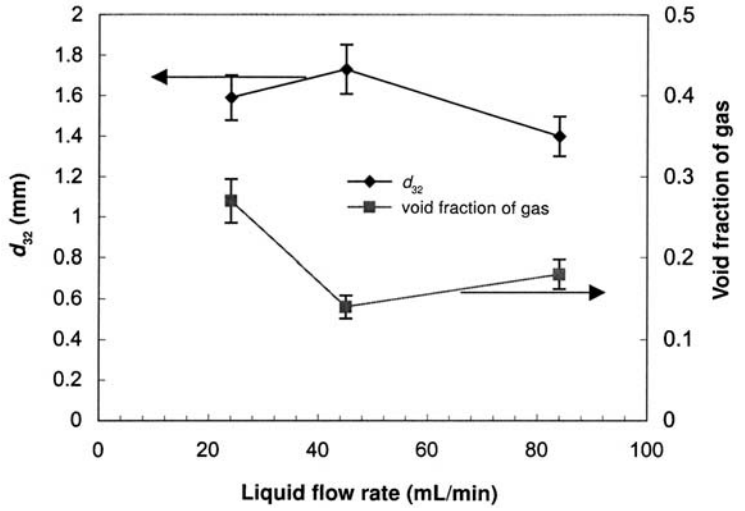

Fig. 11. Bubble size, d_{32}, and void fraction of gas vs liquid flow rate at higher bubble column position (position –1 cm) under initial ovalbumin concentration of 35 mg/L, superficial gas velocity of 0.1 cm/s, and pH 6.5 (original solution).

the surface concentration becomes saturated, the surface tension and the bubble size will no longer change.

Sauter Mean Diameter (d_{32}) and Void Fraction Varied with Superficial Gas Velocity

Figure 10 shows the results of the effect of superficial gas velocity on the bubble size and void fraction at position –12 cm. When the superficial gas velocity increases, the void fraction becomes larger. That follows because the gas flow rate increases as the gas velocity increases for the fixed diameter column and the increased sparging rate leads to a larger void fraction. The bubble size at this position, however, does not change as much with the increase in superficial gas velocity. Tentatively, it can be concluded that the superficial gas velocity is not a significant factor in affecting the bubble size in the lower bubble column (–12 cm). This is in agreement with the observation of Wong et al. *(13)*.

Effect of Feed Flow Rate

Figure 11 shows the effect of feed flow rate on the average bubble size (d_{32}) and void fraction in our experiments. It is seen that the feed flow rate influenced bubble size slightly. The void fraction decreased with an increase in feed flow rate. This is apparently the first time that bubble size and void fraction are investigated subject to the feed flow rate change.

Effect of pH on Bubble Size

Figure 12 shows the effect of pH on bubble size, d_{32}. The *p*I of ovalbumin is about 4.5 *(21)*. From Fig. 12, it is observed that at lower concentra-

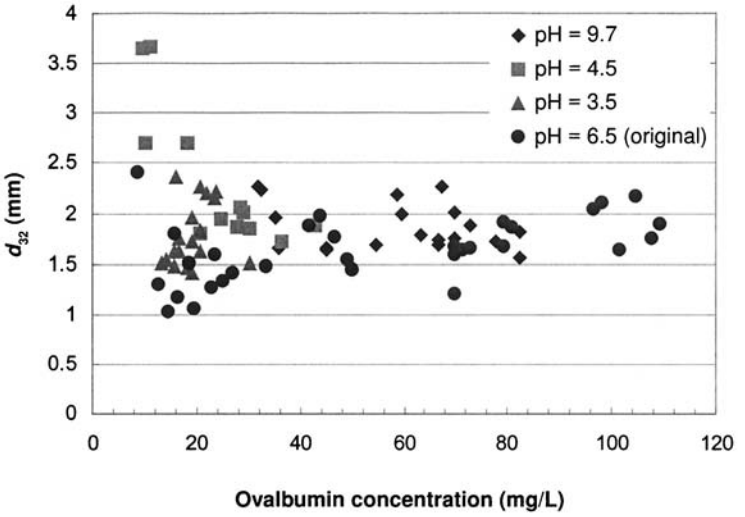

Fig. 12. Effect of pH on bubble size, d_{32}, at an upper position of the bubble column (position –1 cm) at different local ovalbumin concentrations. Other conditions were as follows: superficial gas velocity = 0.1 cm/s and liquid flow rate = 24 mL/min.

tions and pH 4.5, the bubble size is much larger than the average value at other conditions. The surface charge of proteins, which is determined by the solution pH, affects the rheology and stability of bubble films and, thus, the bubble size in the bubble and foam columns. At the *p*I, the net charge of protein molecules is 0 and the electric interaction between them is at a minimum. This may explain the large bubble size when the pH equals the *p*I. The detailed mechanism is not yet clear.

In summary, the bubble size distribution in the bubble and lower position of the foam column obtained is broad. A single average bubble diameter such as d_{32} may be inadequate for representing the bubble size distribution in the column. Because small bubbles control the interfacial area, while large bubbles control the drainage in the foam *(12)*, the bubble size distribution may better characterize the variation in bubble size in the column vs just one average bubble diameter.

Conclusion

The photoelectric capillary probe method was used to measure bubble size distribution, an important descriptive tool in elucidating mechanisms of the foam fractionation process, both in bubble and foam columns. The measurement is interpreted by applying a theoretical pressure calibration to the measured bubble size. For the foam fractionation column studied, a particular funnel-shaped inlet design in the capillary was selected, and a suitable vacuum pressure drop was chosen. The determined bubble size distributions in both the bubble and lower position of the foam columns were obtained with good reproducibility for the ovalbumin foam

fractionation process. The measured bubble size distributions and void fractions are helpful in understanding the foam fractionation process of proteins. Further study is suggested to extend this method for measuring the bubble size at higher positions of the foam column.

Acknowledgment

This work was supported by the National Science Foundation grant no. CTS-9712486.

Nomenclature

A = internal cross-sectional area of capillary tube (m^2)
d_b = bubble diameter (mm)
d_c = inside diameter of capillary (m)
l_b = length of bubble slug (m)
l_c = capillary tube length (m)
p = pressure at detection point of capillary (Pa)
P_A, p_0 = pressure at sampling point of dispersion (Pa)
P_v = pressure at capillary tube outlet, or vacuum pressure (Pa)
S_b = cross-sectional area of a bubble slug (m^2)
S_k = cross-sectional area of a capillary tube (m^2)
t_b^* = time for bubble slug to pass detection point on capillary tube (s)
U_b^* = bubble velocity at detection point (m/s)
V_b = bubble volume in dispersion (m^3)
z = distance between point of observation and outlet of capillary tube (m)
μ = dynamic viscosity (Newton-seconds/m)
ρ = fluid density (kg/m)
σ = surface tension (N/m)

References

1. Greaves, M. and Kobbacy, K. A. H. (1984), *Chem. Eng. Res. Des.* **62,** 3–12.
2. Weiland, P., Brentrup, L., and Onken, U. (1980), *German Chem. Eng.* **3,** 269–302.
3. Barigou, M. and Greaves, M. (1991), *Meas. Sci. Technol.* **2,** 318–326.
4. Gao, D., Xu, Z., and Zhang, J. (1986), *J. East China Inst. Chem. Technol.* **12(Suppl.),** 115–126 (in Chinese).
5. Yu, B., Deng, X., and Shi, Y. (1988), *J. East China Inst. Chem. Technol.* **14(5),** 588–596 (in Chinese).
6. Jiang, H. and Gao, D. (1988), *J. East China Inst. Chem. Technol.* **14(5),** 597–604 (in Chinese).
7. Zhang, Z., Dai, G., and Chen, M. (1989), *J. Chem. Eng. Chin. Univ.* **3(2),** 42–49.
8. Uraizee, F. and Narsimhan, G. (1995), in *Bioseparation Processes in Foods*, Singh, R. K. and Rivzi, S. S. H., eds., Marcel Dekker, New York, pp. 175–225.
9. Uraizee, F. and Narsimhan, G. (1996), *Biotechnol. Bioeng.* **51,** 384–398.
10. Calvert, J. R. and Nezhati, K. (1987), *Int. J. Heat Fluid Flow* **8(2),** 102–106.
11. Magrabi, S. A., Dlugogorski, B. Z., and Jameson, G. J. (1999), *Chem. Eng. Sci.* **54,** 4007–4022.
12. Brown, L., Narsimhan, G., and Wankat, P. C. (1990), *Biotechnol. Bioeng.* **36,** 947–959.

13. Wong, C. H., Hossain, M. D., Stanley, R. A., and Davies, C. E. (1996), in *CHEMECA'96, 24th Australian and New Zealand Chemical Engineering Conference Proceedings*, vol. 4, Sydney, Australia, pp. 105–110.
14. Wilde, P. J. (1996), *J. Colloid Interface* **178,** 733–739.
15. Bae, J. H. and Tavlarides, L. L. (1989), *AIChE J.* **35(7),** 1073–1084.
16. Wallis, G. B. (1969), in *One-Dimensional Two-Phase Flow*, McGraw-Hill, New York, pp. 212–314.
17. Bradford, M. M. (1976), *Analyt. Biochem.* **72,** 248–254.
18. Lage, P. L. C. and Espósito, R. O. (1999), *Powder Technol.* **101,** 142–150.
19. Brown, A. K., Kaul, A., and Varley, J. (1999), *Biotechnol. Bioeng.* **62(3),** 278–290.
20. Tanner, R. D., Parker, T., Ko, S., Ding, Y., Loha, V., Du, L., and Prokop, A. (2000), *Appl. Biochem. Biotechnol.* **84–86,** 835–842.
21. Hammershøj, M., Prins, A., and Qvist, K. B. (1999), *J. Sci. Food Agric.* **79,** 859–868.